A new multicontact tribometer for deterministic dynamic friction identification

J.L. Dion, G. Chevallier, O. Penas, F. Renaud

A new multicontact tribometer for deterministic dynamic friction identification

J.L. Dion *, G. Chevallier, O. Penas, F. Renaud

LISMMA—EA2336, SUPMECA, 3 rue Fernand Hainaut, 93400 SAINT OUEN, France

This paper presents an original friction measurement setup. It is designed to uncouple normal and tangential loads. Friction measures acquired with this setup present a high signal to noise ratio. This friction experimental device allows characterizing various types of surfaces and several levels of excitation from static strain to dynamical motion including micro-sliding and macro-sliding. A measurement example is presented for a contact pair of aluminum alloys starting from sticking limit until complete sliding. Finally, in order to use the results in vibration models, a method is proposed to identify the Lugre Model from these measurements.

1. Introduction

In many studies, the dynamic behavior of a mechanism is only represented through the modeling of each solid in terms of stiffness, mass and damping. However to improve the accuracy of numerical tests, models of mechanisms also have to represent joints between solids. These joints have to model the free relative degrees of freedom (DOF) and the stiffness and the damping in the broad meaning. Joints between solids can be realized by several surfaces (plane, cylinder, sphere, etc.). While nominal topology and geometry of these surfaces determine the kinematic DOF of the perfect joint, their real surfaces, including machining flows (flatness, roughness and so forth) and materials in contact, define their specific stiffness and damping properties.

This paper aims to propose an original tribometer designed in order to improve the quality of friction measurements performed since decades either in our laboratory [1,2] or in previous experimental works [3–6]. The improvements proposed lead to an original structure of the specimens which leads to a normal force independent from the tangential motion. Moreover, as fretting movements are measured, sensors and actuators have been chosen to obtain very accurate results especially for the tangential relative motion. For each pair of surfaces in contact, two main classes of forces can be identified [7]: forces normal to the contact surfaces and friction forces between either sliding surfaces or surfaces assumed to be "clamped" together.

In both cases, these forces introduce energy dissipations that are greater than the intrinsic damping of metallic solids [8,9] and in several applications greater than the damping introduced by polymer materials [10]. However, for many reasons, non-linear behavior, difficulties of identification techniques, etc., this kind of dissipation is sometimes missing in models or wrongly described (for example, by viscous damping models). In fact, in order to predict precisely vibration levels and dynamic behavior of structures and mechanisms, both these forces have to be taken into account before the intrinsic damping of materials [8,9]. From the industrial viewpoint, friction forces are more frequently taken into account, especially in moving mechanisms (such as robots or satellites). Nevertheless, even large assembled structures with bolts, rivets or welding points (such as space launchers and car chassis) are generally assumed to be perfectly clamped; in fact micro-motions and micro-sliding occur between the parts [11]. When surfaces are in contact, which is the case of most mechanisms, tangential forces are often modeled by a Coulomb friction force [7]. For sticking cases, models incorporate kinematic constraints while for slipping cases, they incorporate a constant tangential force between both parts.

In any case, these models need previous measurements on an experimental setup before parametric identification, especially to estimate the friction coefficient. Moreover, to take into account what happened before the complete sliding, other models have been developed with internal state variables that have led to the introduction of micro-sliding [12–15]. All of these models, for instance, Dhal's Model and the LuGre Model, are mathematically very well formulated to be integrated in ODE such as those which govern vibrations. These equations can be solved numerically in time domain [14,15] or analytically [15]. These models are phenomenological and

* Corresponding author. Tel.: +33 1 49 45 29 12; fax: +33 1 49 45 29 69.
E-mail address: Jean-luc.dion@supmeca.fr (J.L. Dion).

Nomenclature

Tangential load F_t, [N]
Normal load F_n, [N]
Normalized sticking stiffness K_0, [m^{-1}]
Normalized sliding stiffness K_1, [m^{-1}]
Sticking stiffness $K_0.F_n$, [N/m]
Sliding stiffness $K_1.F_n$, [N/m]
Real displacement x, [m]
Internal displacement state variable z, [m]
Real velocity $\dot{x}$, [m/s]
Internal velocity state variable $\frac{dz}{dt}$, [m/s]
Friction function $g(\dot{x})$, [dimensionless] ou [N/N]
Dynamic friction factor μd, [dimensionless] ou [N/N]
Static friction factor μs, [dimensionless] ou [N/N]
Transition velocity V_s, [m/s]

semi-empirical with three or more parameters which have to be previously identified with an experimental setup. It is very important to have accurate experimental results to obtain an accurate modeling of the behavior of the corresponding structure. In the present paper, the chosen and identified model is the LuGre model whose parameters are identified from experimental results on the new tribometer described in this paper.

2. Experimental setup

The test bench is designed to characterize the parameters of friction models with an improved accuracy. The quality of measurements is very important for the prediction of complex industrial systems but is often underestimated or obtained with noisy measurements and large uncertainties in parametric identification as shown by Camara M. [2]. So the test bench should allow to ensure good quality of measurements and test conditions over a wide frequency bandwidth.

2.1. Innovative aspects

In previous works, [16,17] for instance, tribometers dedicated to the evaluation of dynamic friction have been developed. Such tribometers aimed to apply and to measure normal force and to control tangential displacement or force. Not only do tangential and normal forces have to be independent, but also the aim of the designers is to measure the coefficient of friction in a frequency range as great as possible and to have the greatest amplitude range in the tangential direction displacement. In [16,17], the tribometers used are the so-called inertial tribometers and are able to ensure a modulation of the normal load less than 1% which is in the same range as for our tribometer. Nevertheless, due to internal resonance, inertial tribometers are generally limited to 100 Hz whereas our tribometer is limited by the MTS hydraulic tester: 200 Hz. Moreover, tangential displacements are generally lower than 1 μm at 40 Hz with inertial tribometers whereas they are greater than 100 μm at the same frequency with our tribometer setup. As a consequence, it is possible to characterize the transient friction coefficient, from sticking to large sliding, with all the partial sliding or micro-sliding steps in a very large frequency bandwidth. These performances allow one to work on dynamic friction coefficient, friction damping or vibrations-induced fretting.

Experiments are often carried out with fretting machines [18,19], pin-on-disc tribometer [20] or directly on specific measuring devices corresponding to the real system under study [1]. Dynamic parameters are mostly identified by a force-deflection loop under harmonic excitation [12]. The test bench proposed has been designed for a wide range of load cases: adjustable static normal force (up to 10 kN), alternative tangential force (up to ± 6 kN), adjustable frequency (up to 200 Hz), with different shapes and materials for surfaces in contact.

Previous experimental works performed [3–5] have revealed the difficulty to measure accurately friction parameters with pin on disc or pin on plane tribometers. Other tribometers have been designed and improved in our laboratory since decades [1,2] to minimize dynamic coupling and uncertainties problems in the measurement of dynamic friction. Measures realized with this kind of tribometers are often noised and biased by dynamic coupling between directions [3], non-deterministic behavior for a unique sample, and localization of remote sensors far from samples [17]. These technological difficulties can lead to systematic errors in parametric identifications. Thus, parameters are also frequently obtained with large uncertainties [2]. Moreover, for several couple of materials each set of pin and plane can lead to different measures according to the reproducibility of the machining process. Uncertain properties of samples induce statistical errors on parameters and several tests have to be carried out in order to reduce this kind of uncertainties. In order to avoid previous cited sources of uncertainties, the new test bench aims to uncouple normal and tangential loads.

Previous studies, [18,19] for example, have been performed with a DN55 tribometer from Phoenix Tribology. The new tribometer is designed for larger static and dynamic loads and for larger specimens. Moreover, with respect to the Abbe principle, most of the sensors have been located close to the contact points and axles of sensors are merged (or close) to the contact displacement axle (see Fig. 3). On the DN55 tribometer, sensors are not so close [18,19]. Based on our knowledge and our experiences in tribometer design, when sensors are not very close to the contacts, different biases are introduced in measures, especially when fretting is performed with high excitation frequencies (more than 50 Hz for example).

Static and dynamic loads allowed on our new tribometer are more than two times greater than those allowed on the DN55 tribometer. The maximum size of specimens is limited to 20 mm on the DN55, whereas specimens larger than 50 mm have been tested on our tribometer.

Moreover, the 16-bit control and data acquisition card used for the displacement control with LVDT sensor on the DN55 do not allow a resolution better than 1 μm. For such small displacements (fretting) at high frequency, a complementary sensor (accelerometer) is needed (see Fig. 3 and Table A1: Ae and Af accelerometers).

Thus, other special hydraulic machines used for elastomeric sample tests at more than 200 Hz are built by MTS (MTS 831.50) and Schenck (VHF7) and designed with LVDT sensors and accelerometers as complementary sensors for hydraulic control in high frequencies.

Finally, the test bench allows to identify the parameters of a realistic lumped model. Furthermore, the LuGre model has been chosen and modified in order to be as elaborated as necessary to be translated into physical sophistications. But the authors have taken care about its usability both to make parametric identification possible on the one hand and for dynamic simulations on the other hand, in a classical framework such as the one presented by D.D. Quinn [21], for instance.

2.2. Description

The test bench should allow to uncouple normal and tangential loads over a wide frequency bandwidth to ensure the good quality of measurements and test conditions, as previously exposed.

In order to verify this assumption and to identify state and rate models, normal force, tangential force, relative displacement and sliding velocity have to be measured over a large frequency range and with a great accuracy.

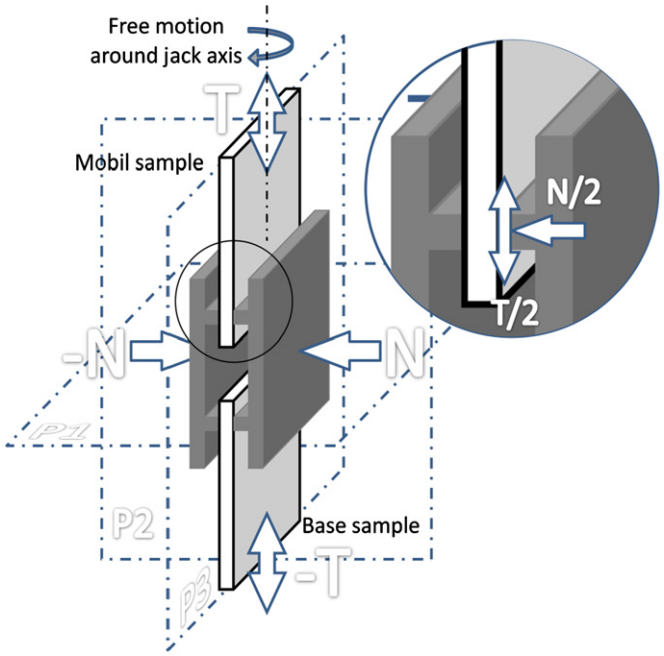

Fig. 1. Principle of contact areas and normal and tangential forces. The three orthogonal symmetry-planes (P1, P2 and P3) allow decoupling between normal and tangential forces and an equal repartition of these forces on each sample.

Our tribometer has been mounted on a MTS Elastomer Test System 830 which allows to obtain at 200 Hz a 1–100 μm displacement range inducing a 1.2–120 mm/s velocity range.

To decouple normal and tangential loads, the test setup is composed of three orthogonal symmetry-planes with four contact areas (Figs. 1 and 3). Each symmetry-plane allows an equal repartition of normal forces (planes P1 and P2) and tangential forces (plane P3). The complete experimental set, composed of samples in the tribometer, is iso-static. The base sample (Fig. 1) is clamped on the reference frame of the hydraulic machine but the mobile sample is free in rotation around the jack displacement axis and avoids hyperstatism in the mechanism. For the same reason, the normal force (N) is performed with a flexible screw. The axis of this screw is placed along the intersection of planes P1 and P2. Moreover, the two application points of the normal force applied by the screw are symmetric on both sides of P3. These technical choices allow to assume a satisfying symmetry for three orthogonal planes, both for geometric properties of the mechanical setup and for load distributions.

Coupling measured between the normal force and the tangential force is shown in Fig. 2 for studied samples (aluminum alloy Al 2017). During the test, with tangential motion, static normal load is assumed to remain static. However the normal load is always measured and controlled with high frequency sampling during the test. This assumption is often not verified on other tribometers. Particular attention has been paid in the design of this tribometer in order to avoid coupling between normal and tangential loads. This coupling is clearly non-linear but does not modify the static normal force over 2% during the tangential dynamic testing as shown in Fig. 2.

The measurement accuracy stems from a high number of samples (four or eight), which allows to measure accurately deterministic behavior and reduces significantly the statistical error. For a single test with linear contact or narrow planar contact, this tribometer uses four sample areas. For a single test with pins on plane or small contact surfaces, this tribometer needs eight sample areas.

In both cases, if possible, samples are machined from a solid block of aluminum alloy, see Figs. 1 and 3. If not, separate samples are clamped with bolts (or screws) and glued with methyl methacrylate adhesive (HBM-X60).

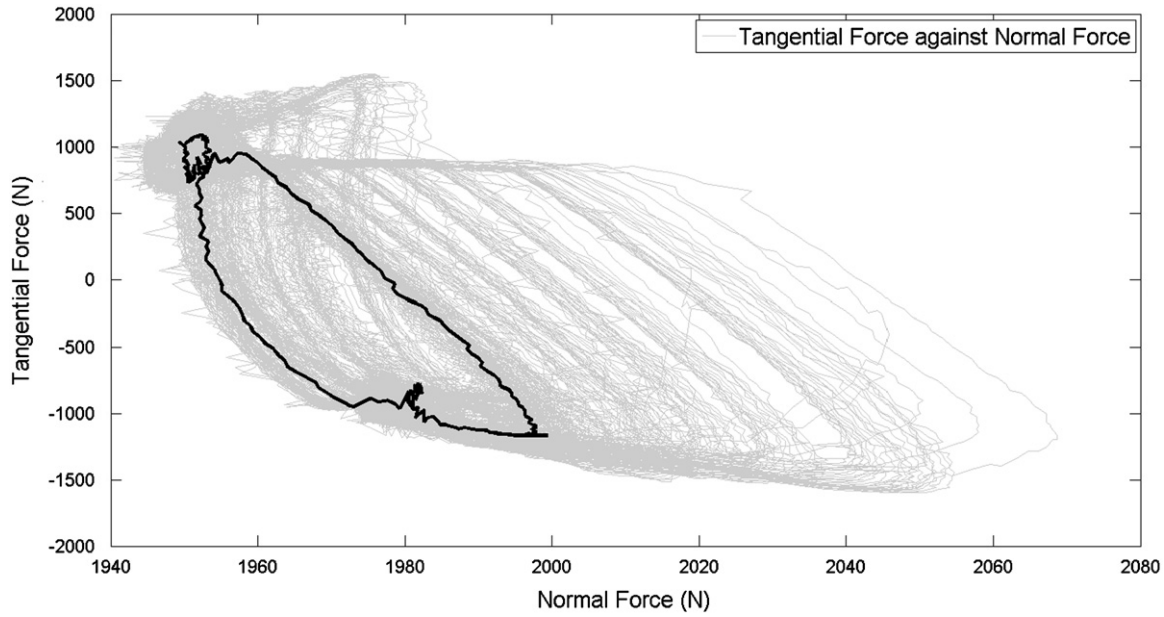

Fig. 2. Coupling between tangential force and normal force—all loops are gray, and one loop is in black for readability. The normal force remains static (2000 N ± 2%) during tangential dynamic testing.

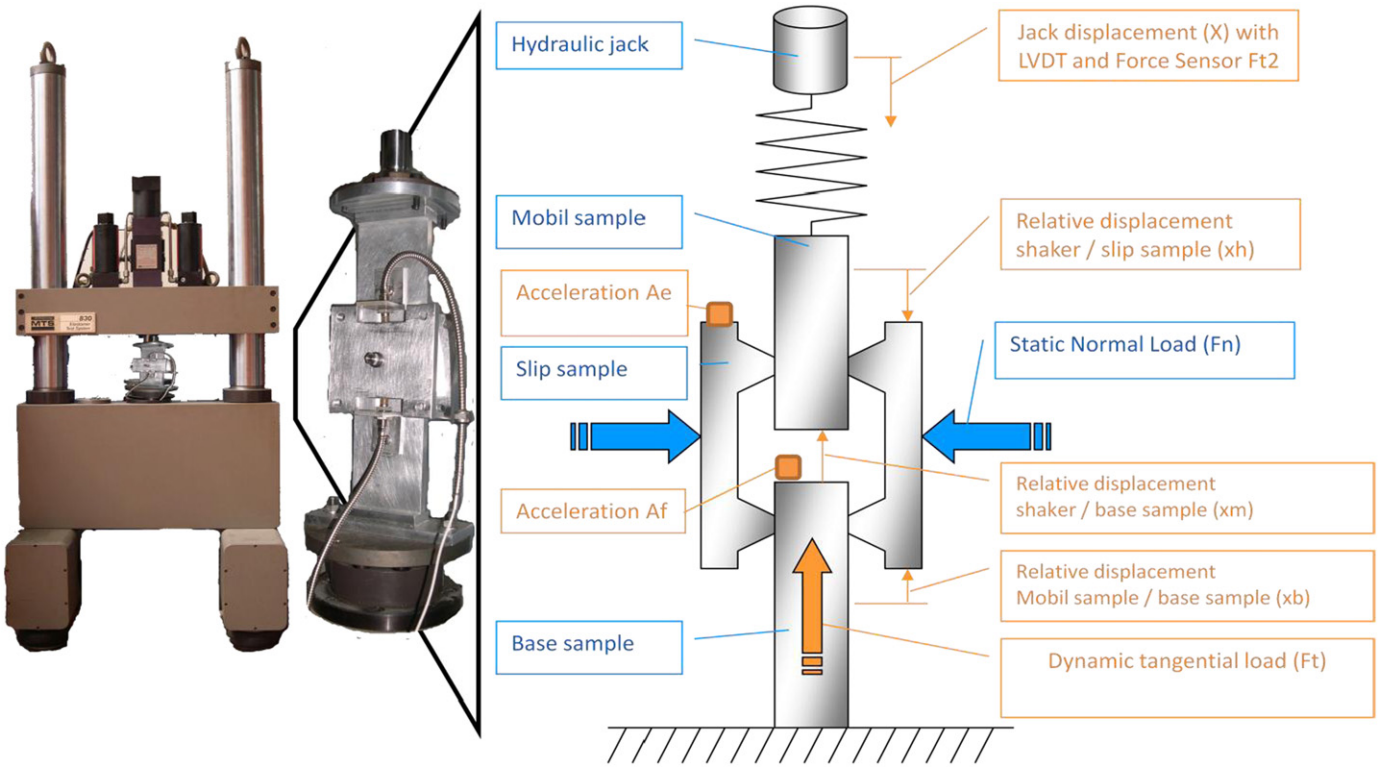

Fig. 3. Schema and partial picture of the tribometer.

2.3. Experimental conditions

2.3.1. Material and specimens

The example used in this study is based on aluminum alloy Al 2017 samples for each contact area.

For the presented experiment and results, each apparent contact surface is a small planar contact designed between 1 cm^2 and 10 cm^2 (Fig. 1). Studied roughnesses are performed by turning, milling or grinding. The examples shown in Sections 2 and 3 are based on samples in aluminum alloy Al 2017 machined by milling. Roughness Ra observed on several samples is between 0.5 and 5 µm and flatness error is lower than 0.02 mm. On the studied samples, effective contact area (measured after the test) is often estimated to 10% of the apparent contact area. Three different sliding conditions have been tested and controlled with sensors. The first condition is performed with no relative displacement between the base sample and slip samples. This condition is obtained with small mechanical stops (groove) on the base sample. The second condition has been performed with the same technique on the mobile sample in order to avoid displacement between the mobile sample and the slip samples. The third test condition is performed without any constraints on the sliding areas (but with a small elastomer link between the base sample and the sliding sample in order to avoid permanent sliding under gravity for very small normal loads). In the limits of our experiences, the three sliding conditions have led to the same numerical results. The choice of four contact areas in the third sliding condition instead of the two proposed on the DN55 is mainly motivated by the desired accuracy in the normal load measurements and in order to avoid coupling between normal and tangential loads.

2.3.2. Load cases

In order to characterize stresses in aerospace assembly, the normal force (F_n) is static between 100 N and 5000 N while the tangential force (F_t) is dynamic between −5000 N and +5000 N. When the four areas are identical (same shape, roughness and surface), the system behaves as if there is only one contact area. However, when the four areas are different, specific properties can be shown (such as dynamic behaviors linked to surface flaws).

The measured forces (normal static force Fn and dynamic tangential force F_t) are composed with two identical forces for each contact area. The normal load is distributed between both contact areas of the same slip sample. Dynamic load is distributed between both contact areas of mobile and base samples. Each contact is loaded with only half of the measured normal load. In the initial analysis, if the friction coefficient is assumed to be independent of the normal force, it can be identified simply by the ratio of tangential force over normal force. Most dynamic friction models assume that forces in action are independent of the real area in contact. In fact, as it can be seen in the last section of this paper, for certain cases this assumption for the contact area is not valid, due to phenomena of local plasticity.

Here, it is assumed that there is no coupling between normal and tangential forces. When the dynamic tangential force is applied, the static normal force keeps its nominal value with a 2% maximum deviation that stems from the dynamic tangential load.

The displacement excitation is controlled and assumed to be sinusoidal. The harmonic ratio (between the fundamental and the 3rd harmonic) is around 5% in the worst cases.

2.3.3. Measurement equipment

For all the tests, hydraulic jack movements are displacement controlled with the feed-back signal of the internal displacement transducer (LVDT).

Measurements are performed with 3 force sensors (F_n, F_t, F_{t2}), 1 LVDT displacement sensor (X), 3 Foucault displacement sensors (xm, xh, xb) and 2 accelerometers (Ae, Af). Most of them are used

in order to verify assumptions, and only 3 sensors are necessary for dynamic friction measurement: 2 force sensors (Ft, Fn) and 1 displacement LVDT (X).

The characteristics of the sensors used are described in Appendix A—Table A1.

2.4. Experimental results and discussion

2.4.1. Force versus displacement and velocity measurements

Forces can be observed versus displacement and velocity. Each type of representation enabling the identification of specific steps and parameters in slipping behavior (Section 3.3) has been selected for the complete parametric identification study. The diagram in Fig. 4 shows the evolution of tangential force Ft versus displacement X. This kind of representation is often used for dissipative behavior. Shape of the curve clearly shows the nature of the behavior (linear or not, dissipative or not, slipping behavior or not, etc.). The area inside the curve is the dissipated energy for one cycle. The quasi-vertical part of the curve represents the system stiffness. The quasi-horizontal part of the curve is the significant behavior of the slip. Most parametric models [22,,23,12,14,15] can be identified with this kind of diagram.

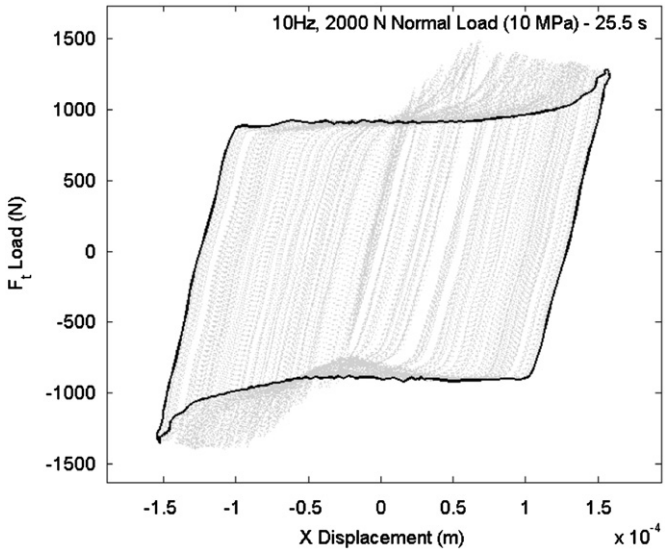

Fig. 4. Slipping behavior under tangential force F_t versus displacement X—all loops with different amplitudes are in gray, and the larger loop is in black.

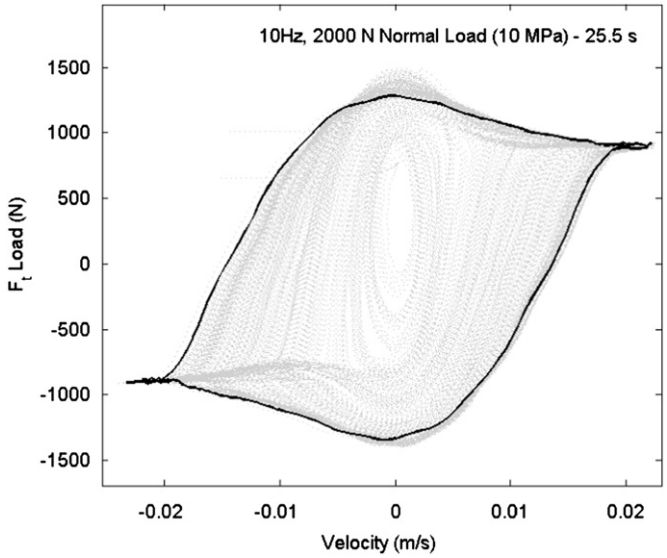

Fig. 5. Slipping behavior under tangential force Ft versus velocity dX/dt with post processing. All loops with different amplitudes are in gray, and the larger loop is in black.

The representation of tangential force versus velocity (Fig. 5) is often used to identify slipping behavior. This chart clearly shows a significant difference between static and dynamic friction coefficients; the tangential force is bigger when the velocity is low (around zero) than when it is higher. Friction coefficients μ are frequently identified with this diagram (Section 3.3). The first cycles of the test show ellipsoid curves that are not representative of slipping behavior. In these particular cases, global slipping does not occur and the behavior is driven by micro-slip and partial slip.

This diagram is also represented in three dimensions as shown in Fig. 6. Instead of tangential load expressed in Newtons, curves can be represented versus the instantaneous friction coefficient (this representation is used in Section 3.3 for parametric identification). Initially, the relation between normal and tangential force is linked to the friction coefficient. For this reason, post-processing with stress (instead of tangential force) was not performed.

2.4.2. Sticking and sliding phenomena: separation of elastic and macroscopic sliding displacements

Displacements due to elasticity and sliding can be separated. The full displacement is measured by using the mobile sample with displacement x (Fig. 3). The sliding displacement is measured by xh (Fig. 7). The elastic displacement xe is computed as the difference between the two previous measurements: $xe = x - xh$. The evolution of the elastic displacement versus sliding displacement highlights the different phases of dynamic friction. In Fig. 7 gray curves represent the whole test and black curve represents only one cycle in four different situations during the test. When sliding occurs, elastic displacement tends to keep constant. Upper and lower limits of this situation are observed with horizontal lines in Fig. 7. Beginning of sliding can be detected on this figure when dynamic cycle (in black) crosses horizontal lines. In the case of oscillations, upper and lower limits are commonly not reached in the same cycle. This situation is obtained for the partial sliding. Macro-sliding cannot be achieved until lower and upper limits were not reached.

First step (Fig. 7, upper left): imposed motion is less than the displacement needed for macro-sliding. Energy losses are due to micro-sliding. Partial sliding is sometimes called mezzo sliding and occurs without any macro-sliding.

Second step (Fig. 7 upper right): imposed motion reaches the sliding limit only in one direction (lower limit on the bottom left of the curve). Partial sliding occurs for a very short time and leads

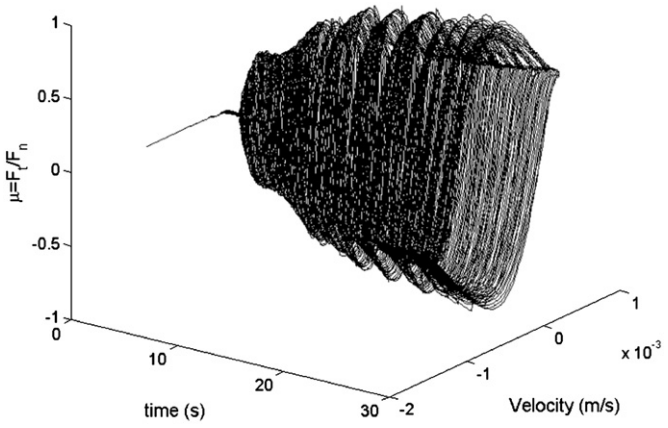

Fig. 6. Instantaneous friction coefficient versus velocity and time.

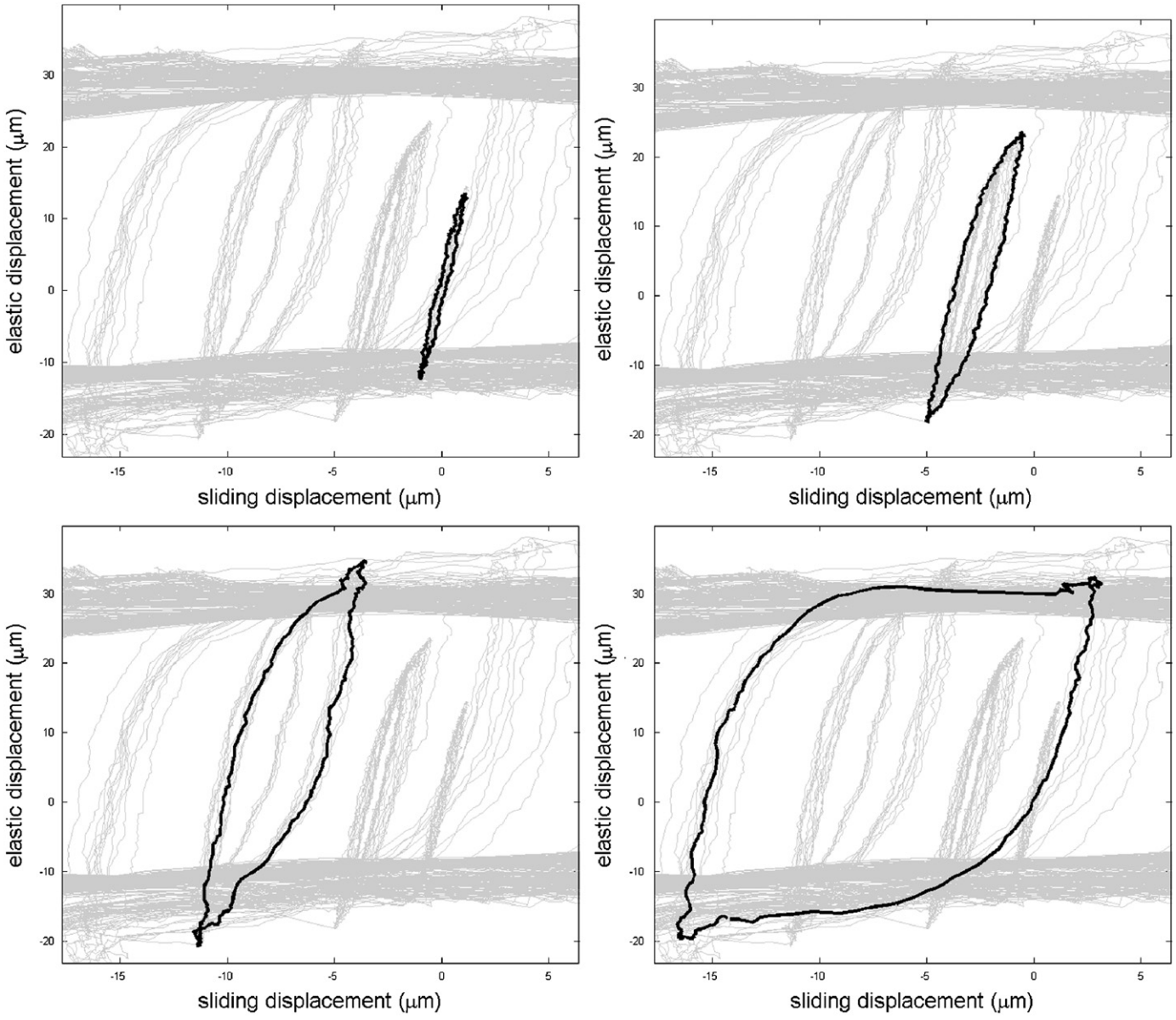

Fig. 7. 4 Steps between sticking and sliding: micro-sliding, partial sliding in one direction, partial sliding in two directions, macro-sliding. Vertical lines are pure sticking with elasticity and horizontal lines are pure sliding. All loops with different amplitudes are in gray, and one loop is in black for each respective step. Sliding displacement is xh (see Fig. 3 Schema and partial picture of the tribometer and elastic displacement is $x_e = x - xh$.

to the decay of displacement signals (simultaneously, signals of tangential load Ft return to being self-centered).

Third step (Fig. 7 lower left): imposed displacement is close to the sliding limit on both directions and macro-sliding has not yet appeared. Upper and lower limits are reached in the same loop. This is the last step before interfaces slide completely, defined as macro-sliding.

Fourth step (Fig. 7 lower right): imposed displacement exceeds the sliding limit in both directions: complete sliding occurs for all cycles.

Fifth step (Fig. 8): imposed motion is much greater than the sliding limit (in both directions): sliding becomes predominant.

The sticking phases are highlighted by the vertical section of the curve: macro-sliding is no longer observed and the entire displacement measured is due to elasticity. The central section of the chart with vertical lines defines two horizontal limits in dashed and dotted lines within which macro-sliding does not exist.

3. Model selection and parametric identification

3.1. Phenomenological models

Several models have been studied in order to describe the dynamic friction observed for aluminum alloy samples. Most dynamic models of frictional behavior are built with internal state variables of kinematic type; however these variables cannot be identified as real physical displacements [1,14,15,22,23]. The first model of this kind was proposed by Dahl [15].

Fig. 9 illustrates differences between several models: Maxwell Slip [7], Dahl [15], Iwan [24], Leuven [25], GMS [22], and LuGre [14]. Regarding experimental results, the GMS and the Lugre Models are the most appropriated models able to describe the Stribeck effect, i.e. the friction force increases when the velocity tends to zero. For samples in aluminum alloy Al 2017 authors have chosen the Lugre model for the parametric identification.

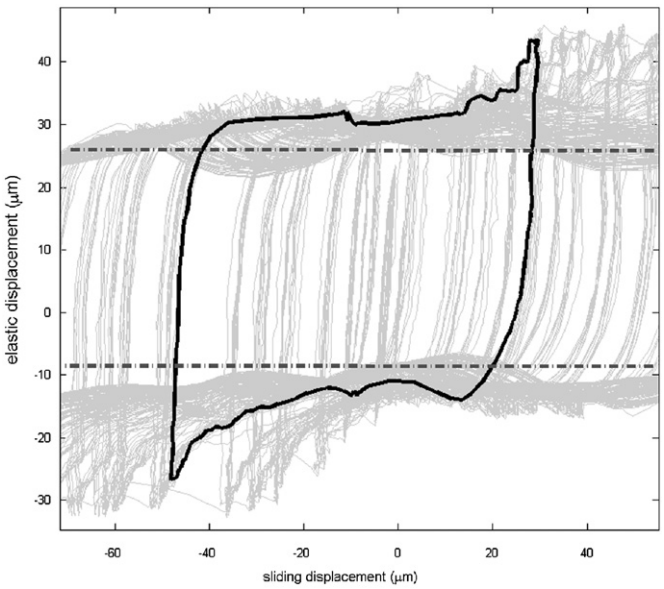

Fig. 8. Macro-sliding: at higher imposed motion the system is driven by sliding. All loops with different amplitudes are in gray, and one loop is in black for step 5.

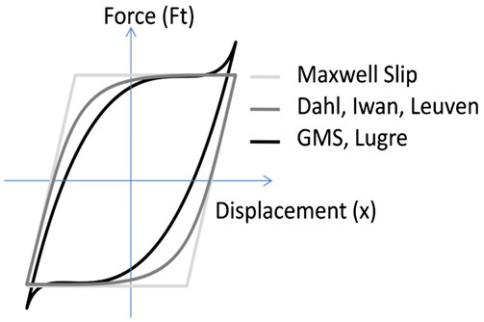

Fig. 9. Sketch of behaviors for several friction models: Maxwell Slip, Dahl, Iwan, Leuven, GMS and LuGre.

The LuGre model [14] can be considered as an evolution of Dahl's model with a velocity dependant friction factor introduced by the "g" function, often chosen as a Gaussian function with $\alpha=2$.

$$\begin{aligned} F_t &= (K_0 z + C_0 \dot{z} + C_1 \dot{x}) F_n \\ \tfrac{dz}{dt} &= \dot{x} - K_0 \tfrac{|\dot{x}|}{g(\dot{x})} z \\ g(\dot{x}) &= \mu_d + (\mu_s - \mu_d) e^{-|\dot{x}/V_s|^{\alpha}} \end{aligned} \tag{1}$$

The LuGre model was completed in 2002 [12] and it includes elastoplastic behavior that occurs before the slipping limit has been reached.

3.2. A rheological approach to the LuGre model

From the viewpoint of modeling friction, the LuGre model (like the Dahl model) can be considered as a non-linear rheological model with linear springs and dampers, and one non-linear damper:

$$\begin{cases} F_t = (K_0.z + C_0.\dot{z} + C_1.\dot{x}) F_n \\ C\{\dot{x}\}.(\dot{x} - \dot{z}) = K_0.z.F_n \\ C\{\dot{x}\} = \tfrac{F_n.g(\dot{x})}{|\dot{x}|} \\ g(\dot{x}) = \mu_d + (\mu_s - \mu_d).e^{-|\dot{x}/Vs|^{\alpha}} \end{cases} \tag{2}$$

This way of modeling allows to quantify the non-linearity of the identified model: particularly for tests with small excitation amplitude, $C\{\dot{x}\}$ can be assumed as a constant (identified with the model linearization).

The two main advantages of this rheological description (Fig. 10) are, firstly, the possibility for future evolutions and combinations of

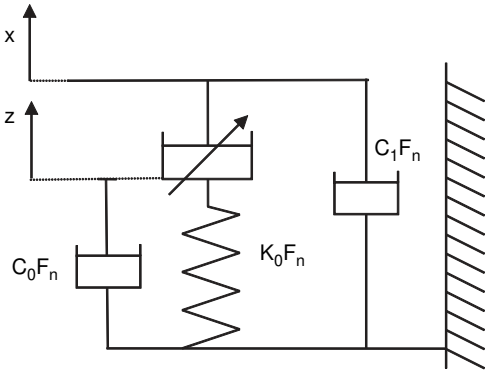

Fig. 10. Rheological description of the LuGre model.

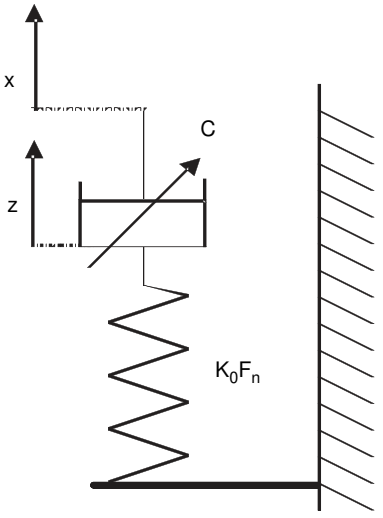

Fig. 11. Rheological description of the model (non-linear Maxwell) used for identification.

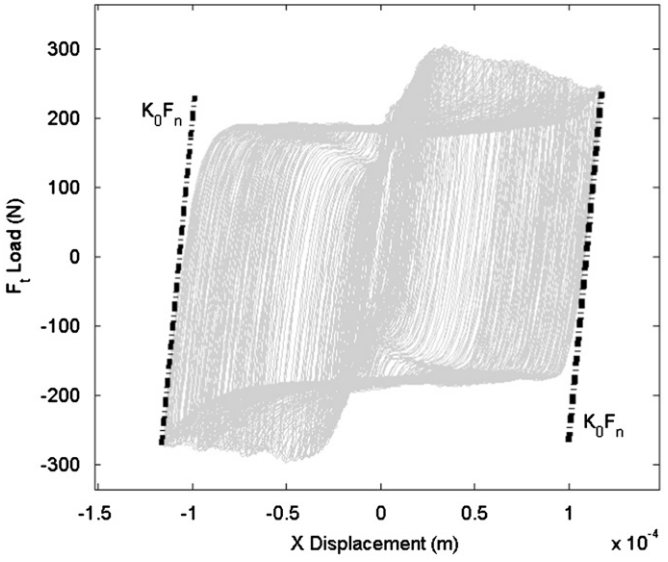

Fig. 12. Stiffness parameter identification.

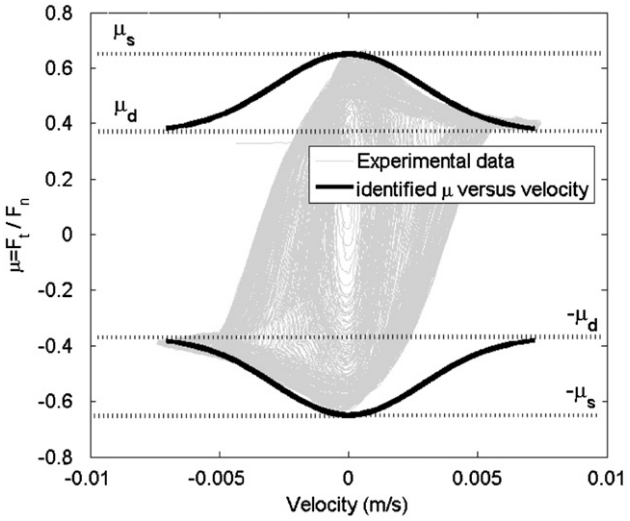

Fig. 13. Friction coefficient identification.

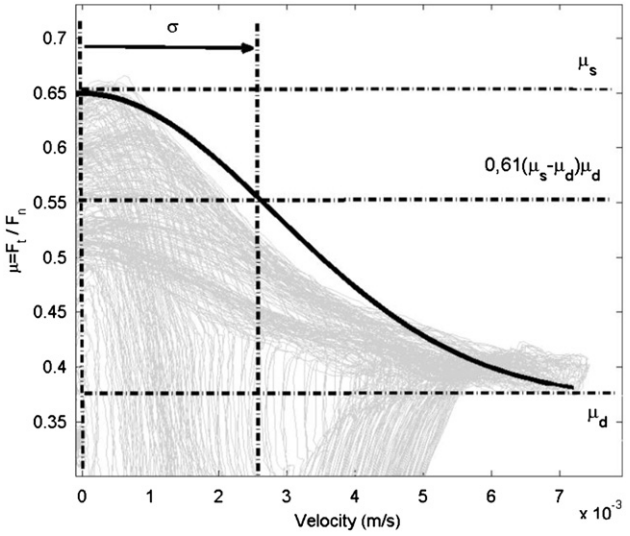

Fig. 14. Transition velocity identification.

the LuGre model with other rheological models, and, secondly, it provides a means for linearizing dissipative behaviors around specific magnitudes of displacement and velocity.

3.3. Parametric identification techniques of the LuGre model

In the studied case, viscous dampers C_0 and C_1, which are designed for fluid behavior, were excluded for metal–metal contact (the main scope of application of this study). The rheological results can be seen as a non-linear Maxwell model (Fig. 11) which can easily fit several friction tests for metal samples.

The parametric identification is based on the subsequent model (Eq. (3)) and represented with a rheological description in Fig. 11: rheological description of the model (non linear Maxwell) used for identification

$$\begin{cases} F_t = K_0.z.F_n \\ C(\dot{x}).(\dot{x}-\dot{z}) = K_0.z.F_n \\ C(\dot{x}) = \frac{F_n.g(\dot{x})}{|\dot{x}|} \\ g(\dot{x}) = \mu_d + (\mu_s - \mu_d).e^{-|\dot{x}/Vs|^{\alpha}} \end{cases} \tag{3}$$

Parametric analyses performed in this study with several samples have shown that the α exponent in the "g" function of the friction coefficient can be set at 2, which is the case of the

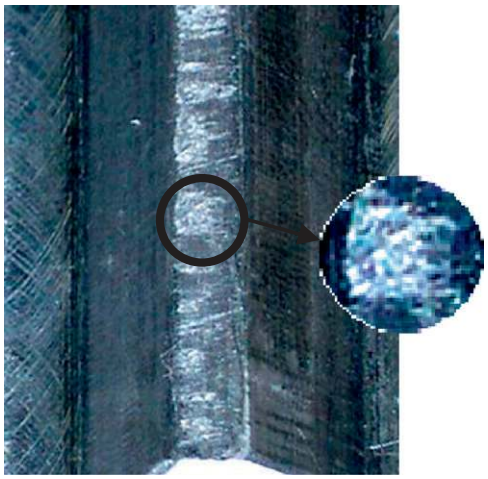

Fig. 16. Damaged tested surface with scoring.

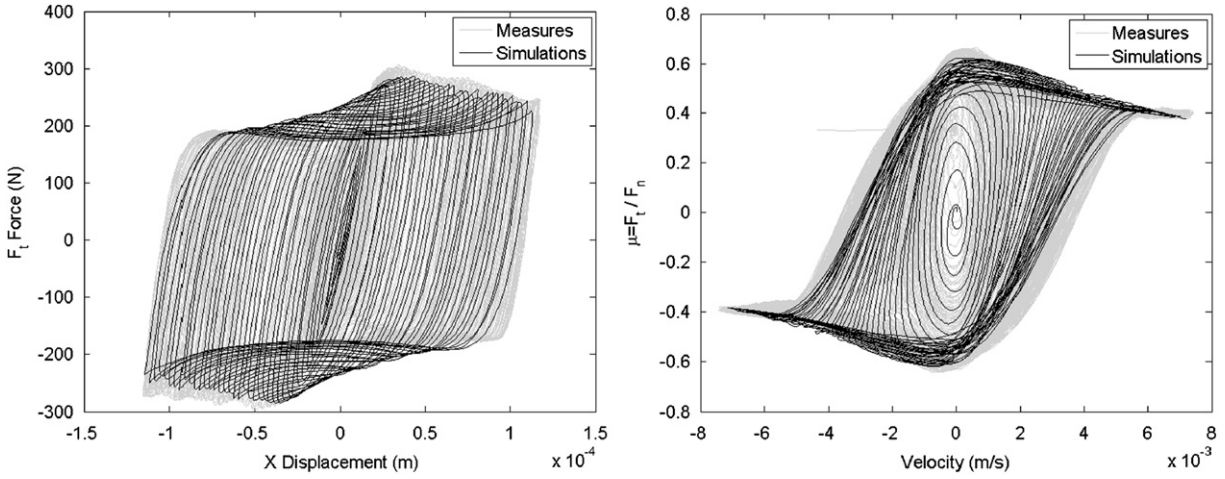

Fig. 15. Comparison between measurement and simulation obtained with the proposed identification method.

Table A1
Characteristics of sensors.

Var.	Sensor principle	Range	S*	E**
F_t	Strain Gauge	−10 kN+10 kN	1 N/mV	< 0.05 % linearity < ± 0.03 % hysteresis
F_n	Strain gauge	0 N–10 kN	1 N/mV	< 0.35 % linearity < ± 0.15 % hysteresis
F_{th}	Strain gauge	−5 kN +5 kN	0.5 N/mV	< 0.05 % linearity < ± 0.03 % hysteresis
x	LVDT	+0,025 m +0,025 m	0.25 mm/V	< 1 % linearity
xh	Eddy current	$+3.10^{-4}$ m $+1.10^{-3}$ m	7 V/mm	< 1 % linearity
xb	Eddy current	$+3.10^{-4}$ m $+1.10^{-3}$ m	7 V/mm	< 1 % linearity
xm	Eddy current	$+3.10^{-4}$ m $+1.10^{-3}$ m	7 V/mm	< 1 % linearity
A_e	Piezoel.	± 500 g	9.93 mV/g	< 1 % linearity
A_f	Piezoel.	± 500 g	9.92 mV/g	< 1 % linearity

S*: sensitivity with associated electronics.
E**: errors (hysteresis, linearity) in % of range.

Gauss function which also offers interesting properties for parametric identification techniques.

This model needs to be previously identified with an experimental test. In that way, this phenomenological model could not be considered as a predictive model. Experimental tests are performed with periodic signals and allow to identify model parameters. However, this model is available for any excitation as random or transient excitations and is used in dynamic simulations.

The prediction of vibration levels is directly linked to the parameters of friction models. In this section the parametric identification method has been built to provide accuracy and can be automatically executed for a broad-based measurement campaign.

Fig. 12 shows tangential load versus displacement as a function of stiffness: the dashed lines with a mostly vertical direction define stiffness K_0 F_n, with Fn the normal load.

The diagram with μ versus velocity (Fig. 13) highlights two friction coefficients: dynamic friction coefficient μd, defined by the limit on the return point corresponding to the maximum speed and static friction coefficient μs, defined by the horizontal tangent around $V=0$.

Transition velocity Vs (Fig. 14) defines the evolution between static and dynamic friction coefficients. The proposed identification technique is based on a property of the Gauss function: for a standard deviation from the median axis, the corresponding value is defined as 61% of the maximum value (on the median axis). This particular point is used to perform σ parameter identification. Parameter σ is identified when the experimental mean of m is equal to $0.61(\mu s-\mu d)+\mu d$. (Curve fitting techniques do not improve significantly the identification.)

$$Vs=\sigma \text{ with } \sigma=V\big|_{\mu=0{,}61(\mu s-\mu d)+\mu d} \tag{4}$$

The proposed identification method is robust and has been applied for a very large number of tests with several frequencies and normal loads. The quality of fitting between simulation and measurements in Fig. 15 is similar for most of the tests; some are better while only a few (less than 5%) are worse.

3.4. Comparison with material data

The static friction factor for this couple of materials in aluminum alloy Al 2017 is usually assumed to be between 0.7 and 1. In the present study, the measured value is 0.7, in accordance with literature [26,27].

When the apparent pressure exceeds 5 MPa, the contact occurring with this material exhibits tribological characteristics [28] that damage the contact area (Fig. 14) instead of reducing roughness in an eroding process similar to that observed for other pairs of materials. Our experimental study was carried out with areas of different sizes and different shapes. When stresses are below the plastic limit of the materials, dynamic and tribological behaviors are independent of the shape or size of the contact area, see [29]. Fig. 16.

4. Conclusion

This work was performed in the field of structural vibrations. In a complex mechanism, the level of vibration strongly depends on the dissipation in the connected parts. This work presents a new test bench designed for improving the accuracy of measurements of non-linear dissipative behaviors of frictional interfaces. This test bench is used for dynamic friction studies. Magnitudes of displacement have been tested from 10^{-5} m to 10^{-2} m while those of velocity have been studied from 10^{-7} m/s to 10 m/s. The tribometer design allows a very good independence between normal and tangential forces. Measurement techniques and signal processing methods highlight excellent accuracy with both direct measurements and parametric identification. As an illustration and because it is very well-formulated for vibrations problems, the LuGre model has been identified from experimental results. An accurate method for parametric identification has been performed and a rheological description of the LuGre model has been presented.

The prospects for improvement of this test means are to enable the measurements of the dissipative behavior on the scale of roughness. Thus the next test bench should make it possible to obtain measurements of displacements under 10^{-7} m.

Appendix A

See Table A1.

References

[1] G. Chevallier, Etude des vibrations de broutement provoquées par le frottement sec—application aux systèmes d'embrayage, UPMC, Paris, 2005.
[2] M. Camara, F. Robbe-Valloire, R. Gras, Y.-M. Chen, Development of a pin-on disc type tribotester in order to study the influence of dynamic load on the tribological behavior, Presses polytechniques et universitaires romandes (2008) 65–74.
[3] K. De Moerlooze, F. Al-Bender, On the relationship between normal load and friction force in pre-sliding frictional contacts part 2: experimental investigation, Wear 269 (2010) 183–189.
[4] D.M. Mulvihill, M.E. Kartala, A.V. Olverb, D. Nowella, D.A. Hills, Investigation of non-Coulomb friction behavior in reciprocating sliding, Wear 271 (2011) 802–816.
[5] M. Eriten, C.-H. Lee, A. Polycarpou, Measurements of tangential stiffness and damping of mechanical joints: Direct versus indirect contact resonance methods, Tribology International 50 (2012) 35–44.
[6] M. Guibert, B. Nauleau, P. Kapsa, E. Rigaud, Design and manufacturing of a recipocating linear tribometer, Tribologie et couplages multiphysiques, Presses polytechniques et universitaires romandes (2008) 55–64.
[7] C.A. Coulomb, Théorie des machines simples, in Mémoires de Mathématique et de Physique de l'Académie des Sciences, 1785, p. 161–335.

[8] N. Makris, S.-P. Chang, Effect of vscous, viscoplastic and friction damping on the response of seismic isolated structures, ISET Journal of Earthquake Technology 35 (4) (1998) 113–141, Paper No. 379.
[9] V. Adams, A. Askenazi, Building Better Products with Finite Element Analysis, OnWord Press, Santa Fe, N.M., 1999.
[10] L. Cremer, M. Heckl, Structure-Borne Sound, Springer-Verlag, New York, 1988.
[11] H. Nouira, E. Foltete, B. Aitbrik, L. Hirsinger, S. et Ballandras, Experimental characterization and modeling of microsliding on a small cantilever quartz beam, Journal of Sound and Vibration 317 (1–2) (2008) 30–49.
[12] A. Almajid, Harmonic response of a structure mounted on an isolator modelled with a hysteretic operator: experiments and prediction, Journal of Sound and Vibration 277 (1–2) (2004) 391–403.
[13] J. Awrejcewicz, C.H. et Lamarque, Bifurcation and Chaos in Non-smooth Mechanical Systems, World Scientific Publishing, J, Singapore, 2003.
[14] C. Canudas de Wit, H. Olsson, K.J. Astrom, P. et Lischinsky, A new model for control of systems with friction, IEEE Transactions on Automatic Control 40 (3) (1995) 419–425.
[15] P. Dahl, A solid Friction Model, The Aerospace Corporation, El Segundo, CA, 1968, TOR-0158H3107–18I-1.
[16] T. Baumerger, L. Bureau, M. Busson, E. Falcon, B. et Perrin, An inertial tribometer for measuring microslip dissipation at a solid–solid multicontact interface, Review of Scientific Instruments 69 (6) (1998) 2416–2420.
[17] V. Lampaert, F. Al-Bender, J. et Swevers, Experimental characterization of dry friction at low velocities on a developed tribometer setup for macroscopic measurements, Tribology Letters 16 (1/2) (2004) 95–105.
[18] X. Huang, R.W. Neu, High-load fretting of Ti–6Al–4V interfaces in point contact, Wear 265 (7–8) (2008) 971–978.
[19] S. Fouvry, P. Duó, P. Perruchaut, A quantitative approach of Ti–6Al–4V fretting damage: friction, wear and crack nucleation, Wear 257 (9–10) (2004) 916–929.
[20] S. Guicciardi, On data dispersion in pin-on-disk wear tests, Wear 252 (11–12) (2002) 1001–1006.
[21] D.D. Quinn, Modal analysis of jointed structures, presented at the IDETC, Washington DC, 2011.
[22] F. Al-Bender, V. Lampaert, J. Swevers, The generalized maxwell-slip model: a novel model for friction simulation and compensation, IEEE Transactions on Automatic Control 50 (N°11) (2005) 1883–1887.
[23] R. Stribeck, Die Wesentlichen Eigenschaften der Gleit – und Rollenlager—the key qualities of sliding and roller bearings, Zeitschrift des Vereines Seutscher Ingenieure 46 (38-39) (1902) 1342–1348.
[24] D.J. Segalman, A four-parameter Iwan model for lap-type joints, Journal of Applied Mechanics 72 (5) (2005) 752–760.
[25] V. Lampaert, J. Swevers, F. Al-Bender, Modification of the Leuven Integrated Friction Model Structure, IEEE Transactions on Automatic Control 47 (4) (2002) 683–687.
[26] M. Szolwinski, Observation, analysis and prediction of fretting fatigue in 2024-T351 aluminum alloy, Wear 221 (1) (1998) 24–36.
[27] J.L. Mo, M.H. Zhu, J.F. Zheng, J. Luo, Z.R. Zhou, Study on rotational fretting wear of 7075 aluminum alloy, Tribology International 43 (5-6) (2010) 912–917.
[28] H. Liu, Tensile properties and fracture locations of friction-stir-welded joints of 2017-T351 aluminum alloy, Journal of Materials Processing Technology 142 (3) (2003) 692–696.
[29] F. Bowden, D. et Tabor, The friction and lubrication of solids, Clarendon Press, Oxford, 1950.